# Multi-input multi-output fuzzy logic controller for utility electric vehicle

BRAHIM GASBAOUI[1], CHAKER ABDELKADER[2], LAOUFI ADELLAH[1]

[1]*Faculty of Sciences and Technology, Department of Electrical Engineering*
*Bechar University*
*B.P 417 BECHAR (08000), Algeria*

[2]*University of ENSET Oran*
*B.P 98 Oran (31000), Algeria*
*e-mail: gasbaoui_2009@yahoo.com*

**Abstract:** Currently commercialization of electric vehicle (EV) is based to minimize the time of starting and acceleration. To undergo this problem multi-input multi-output fuzzy logic controller (MIMO-FLC) affect on propelled traction system forming MMS process was proposed. This paper introduces a MIMO-FLC applied on speeds of electric vehicle, the electric drive consists of two directing wheels and two rear propulsion wheels equipped with two light weight induction motors. The EV is powered by two motors of 37 kilowatts each one, delivering a 476 Nm total torque. Its high torque (476Nm) is instantly available to ensure responsive acceleration performance in built-up areas. Acceleration and steering are ensured by an electronic differential system which maintains robust control for all cases of vehicle behavior on the road. It also allows controlling independently every driving wheel to turn at different speeds in any curve. Direct torque control based on space vector modulation (DTC-SVM) is proposed to achieve the tow rear driving wheel control. The MIMO-FLC control technique is simulated in MATLAB SIMULINK environment. The simulation results have proved that the MIMO-FLC method decreases the transient oscillations and assure efficiency comportment in all type of road constraints, straight, slope, descent and curved road compared to the single input single output fuzzy controller (SISO-FLC).

**Key words:** electric vehicle, electronic differential, space vector modulation, fuzzy logic control, multi-input multi-output fuzzy logic control

## 1. Introduction

Actually, electric vehicle (EV) including, full cell and hybrid vehicle have been developed very rapidly as a solution to energy and environmental problem.

Driven EVs are powered by electric motors through transmission and differential gears, while directly driven vehicles are propelled by in-wheel or, simply, wheel motors [1, 2]. The basic vehicle configurations of this research has two directly driven wheel motors installed and

operated inside the driving wheels on a pure EV. These wheel motors can be controlled independently and have so quick and accurate response to the command that the vehicle chassis control or motion control becomes more stable and robust, compared to indirectly driven EVs. Like most research on the torque distribution control of wheel motor, wheel motors [3, 15] proposed a dynamic optimal tractive force distribution control for an EV driven by four wheel motors, thereby improving vehicle handling and stability [4, 5].

The researchers assumed that wheel motors were all identical with the same torque constant; neglecting motor dynamics the output torque was simply proportional to the input current with a prescribed torque constant.

Direct torque control has become one of the most popular methods of control for induction motor drive systems [8, 13, 17]. DTC can decouple the interaction between flux and torque control, based on both torque and flux instantaneous errors, and provide good torque response in steady state and transient operation conditions. The main advantages of DTC are: absence of coordinate transformation and current regulator; absence of separate voltage modulation block; the actual flux-linkage vector position does not have to be determined, but only the sector where the flux-linkage vector is located, etc. In addition, DTC minimizes the use of machine parameters, so it is very little sensible to the parameters variation [3].

DTC_SVM method is an advanced, computation intensive PWM method and possibly the best among all the PWM techniques for variable speed drives application [19, 21]. Because of its superior performance characteristics, it has been finding widespread application in recent years. With a machine load, the load neutral is normally isolated, which causes interaction among the phases. This interaction was not considered before in the PWM discussion. Recently, fuzzy logic control has found many applications in the past decades, which overcomes these drawbacks. Hence, fuzzy logic control has the capability to control nonlinear, uncertain systems even in the case where no mathematical model is available for the controlled system.

The majority of process industries are nonlinear, multi-input multi-output (MIMO) systems. The control of these systems is met with a number of difficulties due to process interactions, dead time and process nonlinearities [2, 7]. The difference between MIMO systems control and Single-Input Single-Output (SISO) systems control is based on an estimation and compensation of the process interaction among each degree of freedom. It is obvious that the difficulty of MIMO systems control is how to overcome the coupling effects among each degree of freedom. To obtain good performance, coupling effect cannot be neglected. Hence SISO system control scheme is not easy to implement on complicated MIMO systems [8, 9]. In addition, the control rules and controller computation will grow exponentially with respect to a number of considered variables. Therefore, intelligent control strategy is gradually drawing attention.

The structure of the work presented in this paper is organized in the following sequence: The principle components of the Electric traction chain with their equations model is set in Section 2. Section 3 shows the development space vector modulation technique based DTC for Electric vehicle motorization. The proposed structure of the studied propulsion system is given in the Section 4. The simulation results of the different studied cases are presented in Section 5. Finally, the concluding remarks are given in Section 6.

## 2. Electric traction system elements modeling

Figure 1 represents the general diagram of an electric traction system using an induction motor (IM) supplied by voltage inverter [4, 8].
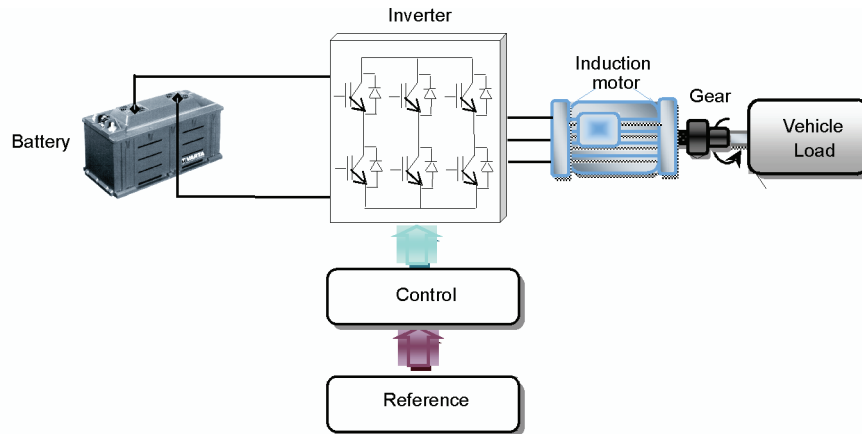


Fig. 1. Electrical traction chain

### 2.1. The vehicle load

The vehicle is considered as a load is characterized by many torques which are mostly considered as resistive torques [4, 5, 16, 17]. The different torques includes:

The vehicle inertia torque defined by the following relationship:

$$T_{in} = J_v \cdot \frac{d\,w_v}{d\,t}.$$     (1)

### 2.2. Aerodynamics fore

This part of the force is due to the friction of the vehicle body, moving through the air. It is q function of the frontal area shape protrusion such as side mirrors ducts and air passages spoilers and any other factor the formula for this component is:

$$F_{\mathrm{aero}} = \frac{1}{2}\rho_{\mathrm{air}} A_f\,C_d v^2.$$     (2)

The aerodynamics torque is:

$$T_{\mathrm{aero}} = \frac{1}{2}\rho_{\mathrm{air}} A_f\,C_d R_w \cdot v^2.$$     (3)

### 2.3. Rolling force

The rolling resistance is primarily due to the traction of the tire on the rode. Friction in bearing and the gearing systems also play their part. The rolling resistance is appositely constant, depend on vehicle speed. It is proportional to vehicle weight the equation is.

$$F_{\text{tire}} = M\,g\,f_r. \tag{4}$$

The rolling torque is:

$$T_{\text{tire}} = M\,g\,f_r\,R_w. \tag{5}$$

### 2.4. Hill climbing force

The force needed to drive the vehicle up a slope is the most straightforward to find it is simply the component of the vehicle weight that acts along the slop. By simple resolution the force we show that [18].

$$F_{\text{slope}} = Mg\sin(\beta). \tag{6}$$

The slope torque is.

$$T_{\text{slpoe}} = Mg\sin(\beta).R_w. \tag{7}$$

We obtain finally the total resistive torque:
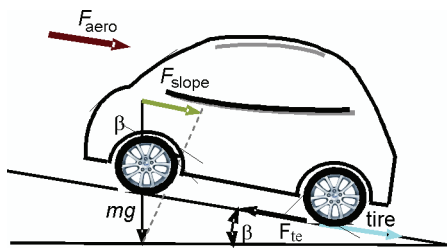


Fig. 2. The forces acting on a vehicle moving along a slope

Where $R_w$ is the tire radius, $M$ is the vehicle total mass, $f_r$ is the rolling resistance force constant, $g$ the gravity acceleration, $\rho_{\text{air}}$ is Air density, $C_d$ is the aerodynamic drag coefficient, $A_f$ is the frontal surface area of the vehicle, $v$ is the vehicle speed, $\beta$ is the road slope angle. Values for these parameters are shown in Table 1.

Table 1. Parameters of the electric vehicle model

| $R_w$ | 0.32 m | $A_f$ | 2.60 m$^2$ |
|---|---|---|---|
| $M$ | 1300 Kg | $C_d$ | 0.32 |
| $f_r$ | 0.01 | $\rho_{\text{air}}$ | 1.2 Kg/m$^3$ |

## 3. Direct torque control using space vector modulation (DTC-SVM)

With the development of microprocessors and DSP techniques, the SVM technique has become one of the most important PWM methods for Voltage Source Inverter (VSI) since it gives a large linear control range, less harmonic distortion, fast transient response, and simple digital implementation [21-22].

The induction motor stator flux can be estimated by

$$\phi_{ds} = \int_0^t (V_{ds} - R_s\, i_{ds})\, dt, \qquad (8)$$

$$\phi_{qs} = \int_0^t (V_{qs} - R_s\, i_{qs})\, dt, \qquad (9)$$

$$|\phi_s| = \sqrt{\phi_{ds}^2 + \phi_{qs}^2}. \qquad (10)$$

And electromagnetic torque $T_{em}$ can be calculated by

$$T_{em} = \frac{3}{2} p (\phi_{ds}\, i_{qs} - \phi_{qs}\, i_{ds}). \qquad (11)$$

The SVM principle is based on the switching between two adjacent active vectors and two zero vectors during one switching period. It uses the space vector concept to compute the duty cycle of the switches. Fig. 4 shows a scheme of a three-phase two-level inverter with a star-connection load.

From Fig. 3, the output voltages of the inverter can be composed by eight states $u_0$, $u_1$ … $u_7$, corresponding to the switch states $S_0(000)$, $S_1(100)$, $S_7(111)$, respectively. These vectors can be plotted on the complex plane ($\alpha\,\beta$) as shown in Fig. 4, and are given by [3].

$$u_k = \begin{cases} \dfrac{2}{3} V_{dc}\, e^{j(k-1)(\pi/3)} & \text{for} \quad k = 1, 2, \dots 6 \\ 0 & \text{for} \quad k = 0, 7. \end{cases}$$

The rotating voltage vector within the six sectors can be approximated by sampling the vector and switching between different inverter states during the sampling period [22]. The vector $u_s$ is commonly split into two nearest adjacent voltage vectors and zero $u0$ and $u7$ in an arbitrary sector. For example, during one sampling interval, vector $u_s$ in sector I can be expressed as

$$u_s(t) = \frac{T_0}{T_s} u_0 + \frac{T_1}{T_s} u_1 + \frac{T_2}{T_s} u_2 + \frac{T_7}{T_s} u_7, \qquad (12)$$

where $T_0$, $T_1$, $T_2$, $T_7$ are the turn-on time of the vectors $u_0$, $u_1$, $u_2$, $u_7$ and $T_s$ is the sampling time.

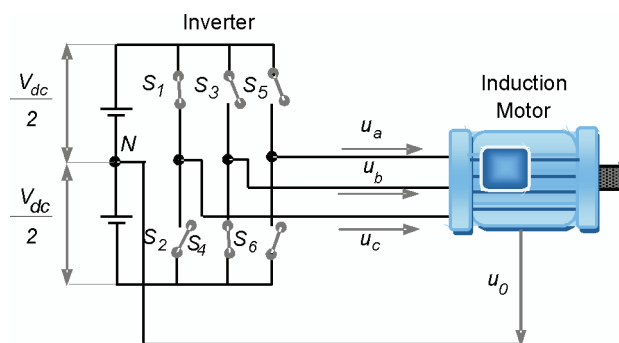$$T_s - T_1 - T_2 = T_0 + T_7 \geq 0, \ T_0 \geq 0, \ T_7 \geq 0.$$



Fig. 3. Three-phase two-level inverter

The block diagram of the DTC-SVM control scheme for voltage source inverter-fed IM is shown in Figure 3. In this method two PI controllers are used for torque and flux regulation. The outputs of the PI flux and torque controllers generate the reference stator voltage components $u_{qs}$, $u_{ds}$ expressed in the stator flux oriented coordinates ($d - q$). These components are *dc* voltage commands and then transformed into stationary coordinates ($\alpha - \beta$) The commanded values $u_{s\alpha}$, $u_{s\beta}$ are delivered to space vector modulator (SVM), which generates switching signals $S_a$, $S_b$, $S_c$ for power transistors [23-24].

We can calculate $u_{ds}^*$ and $u_{qs}^*$ by the following equations:

$$u_{ds}^* = \left( K_{p\phi} + \frac{K_{i\phi}}{s} \right)\left( \varphi^* - \phi \right), \tag{13}$$

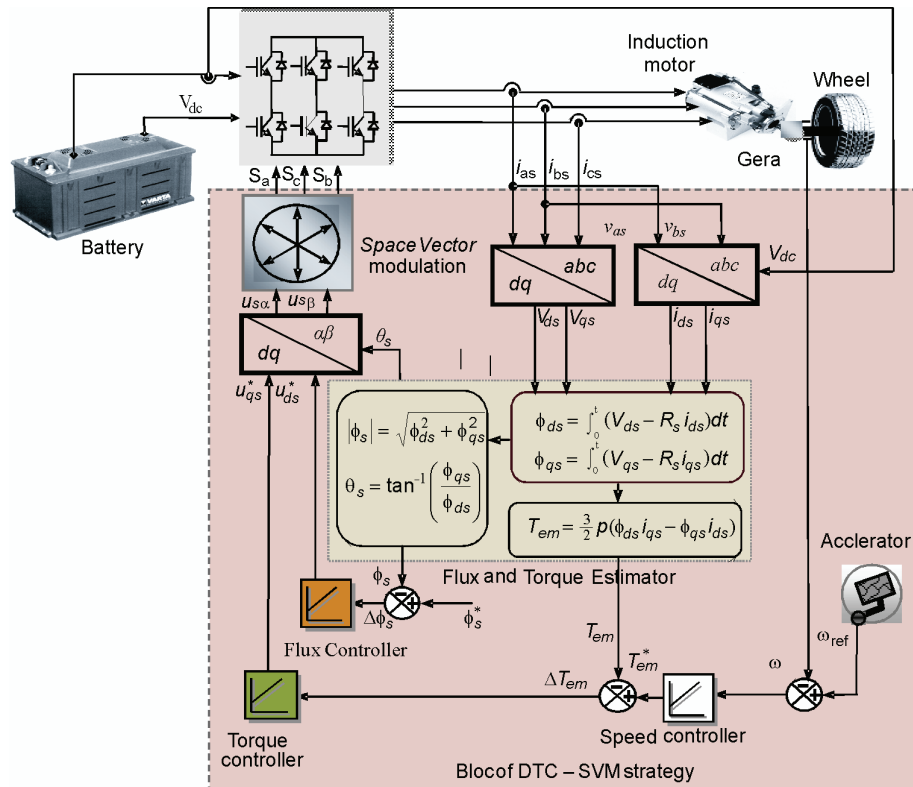$$u_{qs}^* = \left( K_{pT_{em}} + \frac{K_{iT_{em}}}{s} \right)\left( T_{em}^* - T_{em}^* \right). \tag{14}$$



Fig. 4. Three-phase two-level inverter

## 4. Multi-input multi-output fuzzy controller structure

Fuzzy set theory has been successfully applied in a number of control applications [8, 12, 27-30] based on the SISO system point of view without system model consideration. In this

paper, the MIMO fuzzy control strategy is used to multi-machines system speeds control. The block diagram of the MIMO fuzzy control scheme is shown in Figure 5. The design procedure of the fuzzy control strategy is used to control each degree of freedom of this MIMO system individually. Then, an appropriate coupling fuzzy logic controller (FLC) is designed to compensate for the coupling effects of system dynamics among each degree of freedom.

An ordinary fuzzy controller that usually operates with system output error and error change was chosen as the main controller to control each degree of freedom of the MIMO systems. Here, the input variables of the conventional fuzzy controller for among each degree of freedom of a MIMO system were defined individually as:

$$e_i(k) = \omega_i^*(k) - \omega_i(k), \tag{15}$$
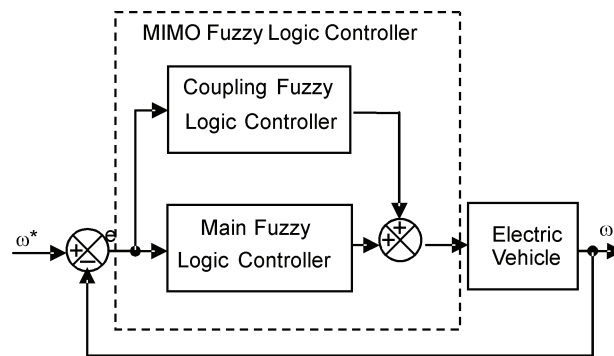
$$\Delta e_i(k) = e_i(k) - e_i(k-1). \tag{16}$$



Fig. 5. Bloc diagram of the MIMO fuzzy control schema

Where $e_i(k)$ is the position error of the $i^{th}$ degree, $\Delta e_i(k)$ is used for change in error of the $i^{th}$ degree, $\omega^* e_i(k)$ is the reference input (Rotation speed reference of the roller i) of the $i^{th}$ degree and $\omega e_i(k)$ represents the $i^{th}$ position output of each degree of freedom (real Rotation speed of the roller i) of this MIMO system at the $k^{th}$ sample. The relationship between the scaling factors $(G_e, G_{\Delta e}, G_u)$ are the input and output variables of the FLC.

$$e_{iN} = G_e \times e_i, \Delta e_{iN} = G_{\Delta e} \times \Delta e_i, \Delta u_i = G_{\Delta u} \times \Delta u_{iN}. \tag{17}$$

Selection of suitable values for $G_e$, $G_{\Delta e}$ and $G_u$ are made based on the knowledge about the process to be controlled and sometimes through trial and error to achieve the best possible control performance. This is so because, unlike conventional no fuzzy controllers to date, there is no well-defined method for good setting of scaling factor's for FLC's. The SFs are the significant parameters of FLC because changing the SFs changes the normalized universe of discourse, the domains, and the membership functions of input/output variables of FLC. All membership functions (MFs) for controller inputs ($e_i$ and $\Delta e_i$) and incremental change in controller output ($\Delta u_i$) are defined on the common normalized domain (Per Unit) $[-1, +1]$. We use symmetric triangles (except the two MFs at the extreme ends) with equal base and

50% overlap with neighboring MFs as shown in Fig. 6. This is the most natural and unbiased choice for MFs. By way of the above design process, the actual control input voltage for the main fuzzy controller can be written as:

$$u_i(k) = u_i(k-1) + \Delta u_i(k). \tag{18}$$

In (24), $k$ is the sampling instant and $\Delta e_i(k)$ is the incremental change in controller output, which is determined by the rules of the form (IF-THEN) If $e_i$ is $E_i$ and $\Delta e_i$ is $\Delta E_i$ Then $\Delta u_i$ is $\Delta U_i$. The rule base for computing is a standard one [8, 12, 29] as shown in Table 2.
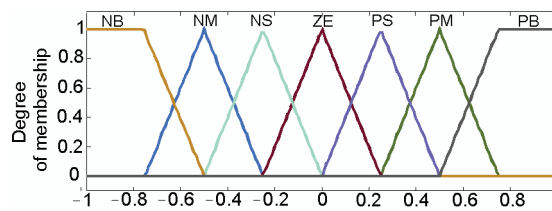


Fig. 6. Membership functions for $e_i$, $\Delta e_i$, and $\Delta u_i$

Where: **NB** – Negative Big, **NM** – Negative Medium, **NS** – Negative Small, **ZE** – Zero Error, **PS** – Positive Small, **PM** – Positive Medium, **PB** – Positive Big.

Table 2. Rules base

| $e_i$ \ $\Delta e_{il}$ | NB | NM | NS | ZE | PS | PM | PB |
|---|---|---|---|---|---|---|---|
| NB | NB | NB | NB | NM | NS | NS | ZE |
| NM | NB | NM | NM | NM | NS | ZE | PS |
| NS | NB | NM | NS | NS | ZE | PS | PM |
| ZE | NB | NM | NS | ZE | PS | PM | PB |
| PS | NM | NS | ZE | PS | PS | PM | PB |
| PM | NS | ZE | PS | PM | PM | PM | PB |
| PB | ZE | PS | PS | PM | PB | PB | PB |

The fuzzy control rules of the coupling fuzzy controller are similar to the main fuzzy controller. The output of the coupling fuzzy controller is chosen directly as the coupling control input voltage. The main reason is that there is a different coupling effect for each sampling interval and it does not have an accumulating feature. The coupling effect is incorporated into the main fuzzy controller for each step to improve system performance and robustness. Figure 7 illustrates the structure of MIMO fuzzy control scheme. Therefore, the total control input voltage of the MIMO fuzzy controller is represented as:

$$u_i(k) = u_i(k) + U(k)_{i \rightarrow l}, \quad i \neq l, \tag{19}$$

where $u_i(k)$ expresses the system control input voltage of the $i^{th}$ degree of a main fuzzy controller. $U(k)_{l \to i}$ represents the coupling effect control of the $l^{th}$ degree relative to the $i^{th}$ degree of the coupling fuzzy controller.
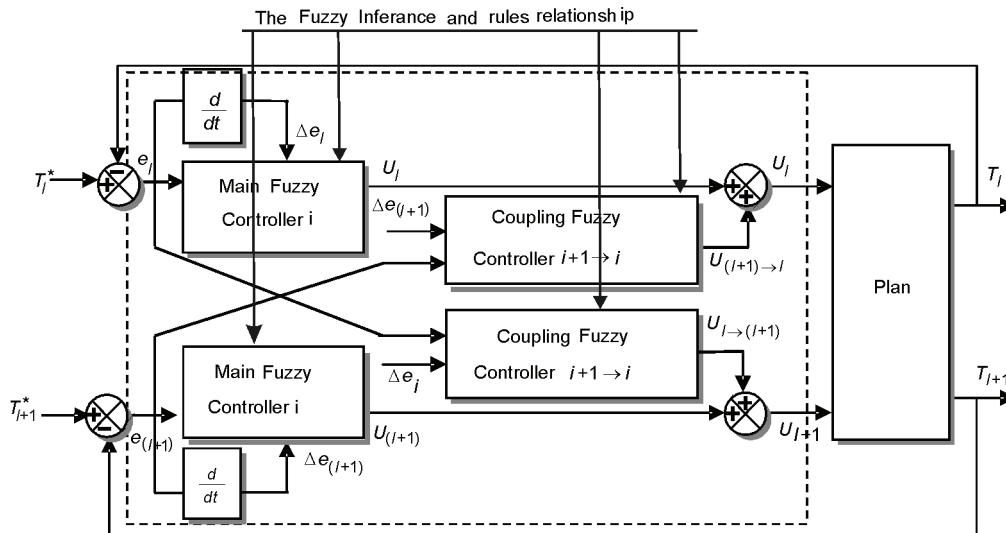


Fig. 7. Structure of MIMO fuzzy control scheme

# 5. Electric differentials and it implementation

The main of the control system should be summarized as follows:

1) A speed network control is used to control each motor torque;

2) The speed of each rear wheel is controlled using speed difference feedback. Since the two rear wheels are directly driven by two separate motors, the speed of the outer wheel will need to be higher than the speed of the inner wheel during steering maneuvers (and vice-versa). This condition can be easily met if the speed estimator is used to sense the angular speed of the steering wheel. The common reference speed $\omega_{ref}$ is then set by the accelerator pedal command. The actual reference speed for the left drive $\omega^*_{left}$ and the right drive $\omega^*_{right}$ are then obtained by adjusting the common reference speed $\omega^*$ using the output signal from the DTC-SVM speed estimator. If the vehicle is turning right, the left wheel speed is increased and the right wheel speed remains equal to the common reference speed $\omega^*$. If the vehicle is turning left, the right wheel speed is increased and the left wheel speed remains equal to the common reference speed $\omega^*$ [7, 9, 11].

Form the model Figure 9, the following characteristic can be calculated:

$$R = \frac{L_w}{tg(\delta)}, \tag{20}$$

where $\delta$ is the steering angle. Therefore, the linear speed of each wheel drive is given by

$$\begin{cases} V_1 = \omega_v \left( R - d_w/2 \right) \\ V_2 = \omega_v \left( R - d_w/2 \right) \end{cases} \tag{21}$$

And their angular speed by

$$\begin{cases} \omega_{rm}^* = \dfrac{L_w - (d_w/2)\tan(\delta)}{L_w}\, \omega_{rm} \\ \omega_{lm}^* = \dfrac{L_w - (d_w/2)\tan(\delta)}{L_w}\, \omega_{lm} \end{cases}, \tag{22}$$

$$\Delta\omega = \omega_{rm}^* - \omega_{lm}^* = -\frac{d_w \tan(\delta)}{L_w}\, w_v. \tag{23}$$

Where $w_v$ is the vehicle angular speed according to center of turn. The difference between wheel drive angular speeds is then and the steering angle indicates the trajectory direction.

$$\delta > 0 \Rightarrow \text{Turn left}, \tag{24}$$

$$\delta = 0 \Rightarrow \text{Straight ahead}, \tag{25}$$

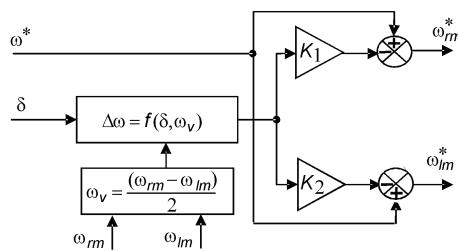$$\delta < 0 \Rightarrow \text{Turn right}. \tag{26}$$



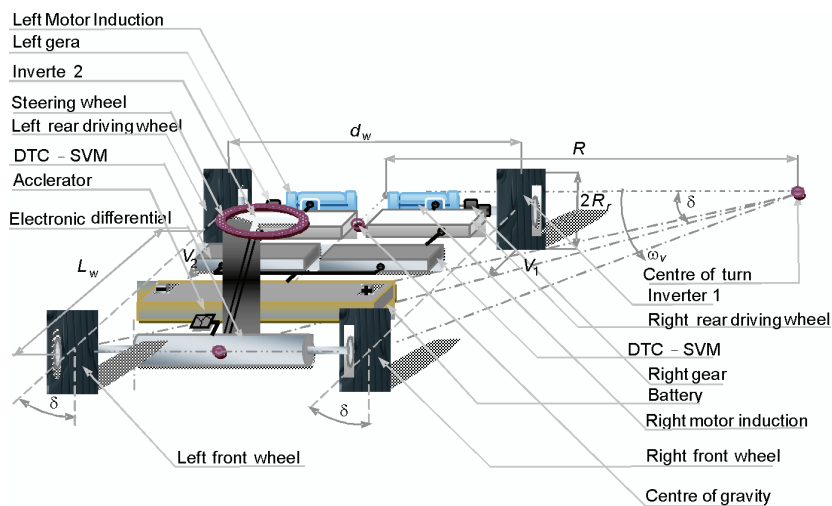Fig. 8. Bloc diagram of the differential system
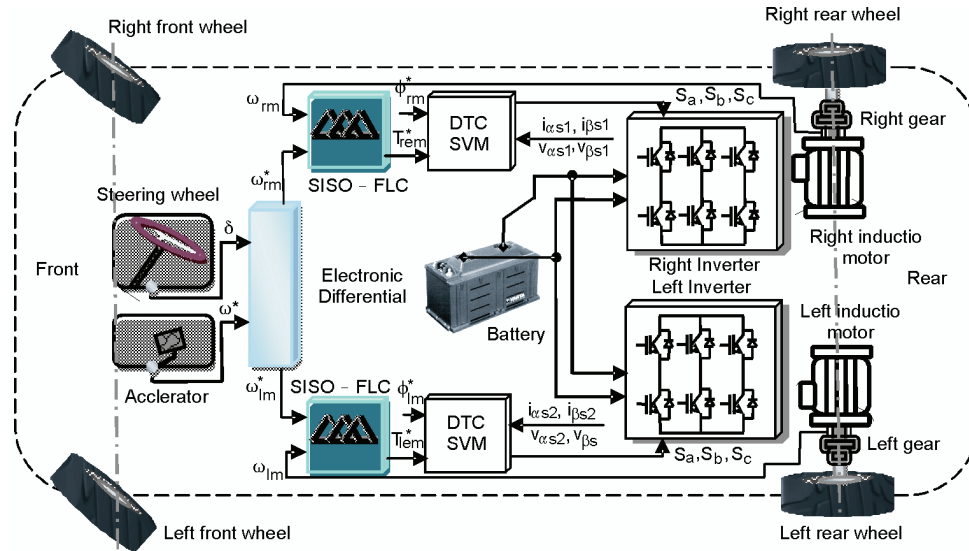


Fig. 9. Structure of vehicle in curve

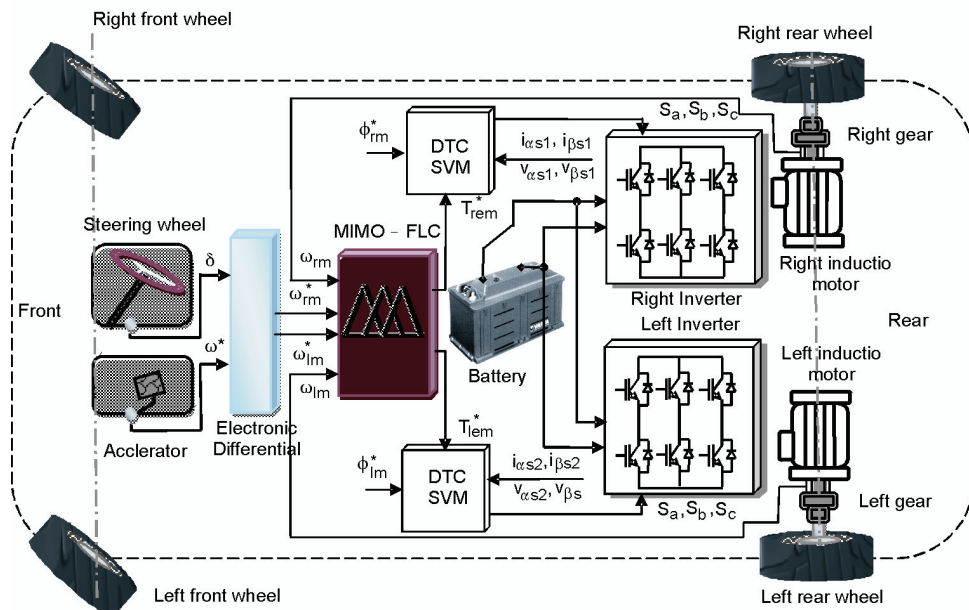Fig. 10. The Driving wheels system with MIMO controller



Fig. 11. The Driving wheels system with SISO controller

## 6. Simulation results

In order to characterize the driving wheel system behavior, Simulations were carried using the model of Fig 10. The following results were simulated in MATLAB and its divided in four

cases, case 1 (acceleration), case 2 (the electric vehicle is moving hill climbing), case 3 (the electric vehicle is moving in straight road) and finally (the electric vehicle is moving down climbing). The specified road topology is shown in Fig. 12.
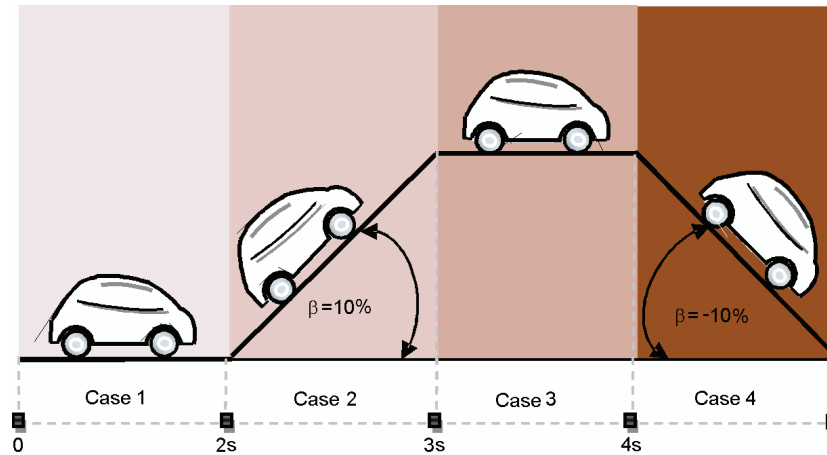


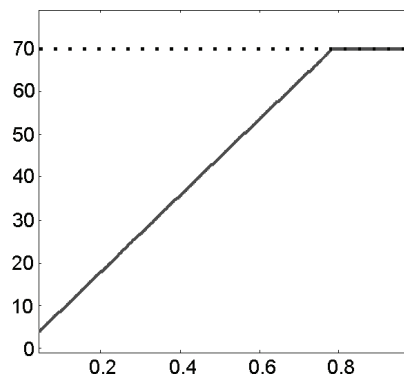Fig. 12. Different trajectory driving by electric vehicle



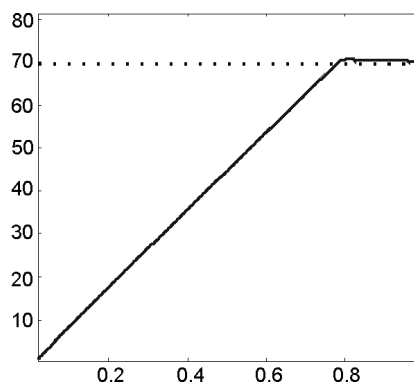Fig. 13. Zoomed of the vehicle speed response with (MIMO-FLC). Speed controller



Fig. 14. Zoomed of the vehicle speed response with (SISO-FLC). Speed controller
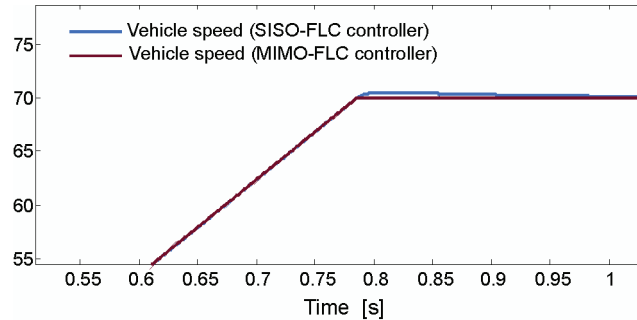
Fig. 15. Zoomed of vehicle speed for two controller cases

To compare the effect of disturbances on the vehicle speed in the cases of two types of control, Figure 15 shows the system response in two cases (MIMO-FLC, and SISO-FLC). We can summaries the vehicle speed results in the following tables:

Table. 3. Performances of the MIMO-FLC & SISO-FLC in the speed loop response



| Results | Overshoot [%] | Rising time [sec] | Overshoot [%] |
|---|---|---|---|
| SISO-FLC | 0.5600 | 0.7087 | 1.0182e + 001 |
| MIMO-FLC | 0.0143 | 0.7073 | 6.8543e + 000 |

According to Figure 15 and Table 2, we can say that the effect of the disturbance is neglected in the case of the MIMO-FLC. It appears clearly that the classical control with SISO-FLC is easy to apply. However the control with MIMO-FLC offer better performances in the rising time control and overshoot. In addition to these dynamic performances, it respects the imposed constraints by the driving system such as the robustness of parameter variations.

**Case 1: (acceleration phases)**
At $t$ = 1 s, the vehicle speed pass from the reference speed of 70 km/h to another reference of 80 km/h, the behavior of these speeds is given by Fig. 15. The electromagnetic torque and current growth sharply. The driving wheels speeds stay always the same and the road slope does not affect the control of the wheel and the MIMO-FLC act immediately on the speed loop's and rejects the disturbance and give's more and more efficiency to the electronic dif-

ferential output references. We can say the slope sensitize the motorization to develop efforts in order to satisfy the electric traction chain demand.
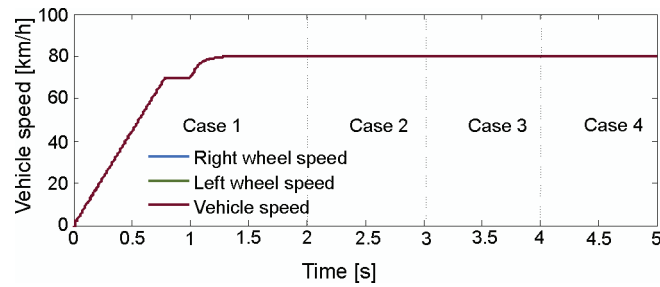


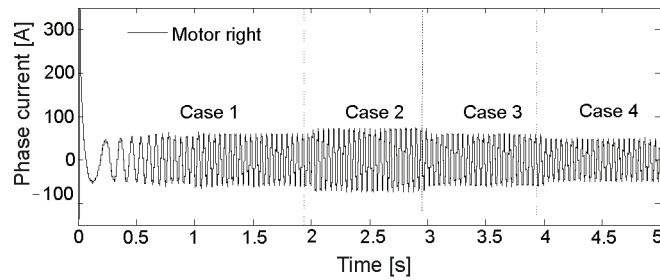Fig. 16. Vehicle wheel speed in different cases



Fig. 17. Variation of phase current for motor right
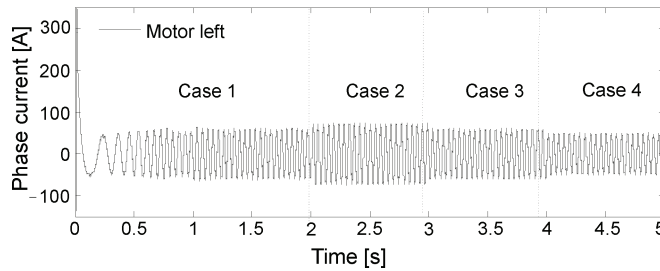


Fig . 18. Variation of phase current for the motor left

**Case 2: (hill climbing)**

At 1 s < $t$ < 2 s this test explain the direct slope effect on the EV. The driving wheels linear speeds stay the same and the road drop does not influence the torque control of each wheels. The both of the back motors develop more and more electromagnetic torque for passing the slope. The behavior of these speeds is given by Figure 15. The variation of electromagnetic torques are illustrated in Figure 19. The presence of slope causes a large increase in the phase current for the right and left motor, and the speed maintain to 80 km/h. The two motors absorb

more energy. The current demand increases and the vehicle can pass the slope easily, the EV torque jumps back to 169 Nm.

**Case 3: (straight road)**

At 3 s < *t* < 4 s the EV are driving in straight road with constant speed, A good tracking of the speed step can be observed in figure 8.2. EV reaches constant speed 80km/h. Delay in reaching this speed follows from acceleration of the vehicle mass. Figures 17 and 18 describe the variation of phase currents for each motor.

**Case 4: (down climbing)**

At 4 s < *t* < 5 s, this test justify the inverse slope on the EV behavior moving on straight road. The presence of descent causes a great decrease in the phase current of each motor, as shown in Figures 17 and 18. The right and left motor are relieved. The both motors develop approximately 350.80 N/m. The MIMO-FLC speed controllers ensure the stability of the propulsion system by maintaining the motorization error speed equal zeros and gives a good rising time, the variation of the electromagnetic torques and vehicle torques are illustrated in Figures 19 and 20 respectively. The presence of descent causes a great decrease in the phase current of each motor by means that the aerodynamic force became a motor force and the other resistive torques became motor torque and the kinetic energy given to the vehicle help the battery in order to charge the empty battery cells. For that the EV torque reach to 86.99 Nm.
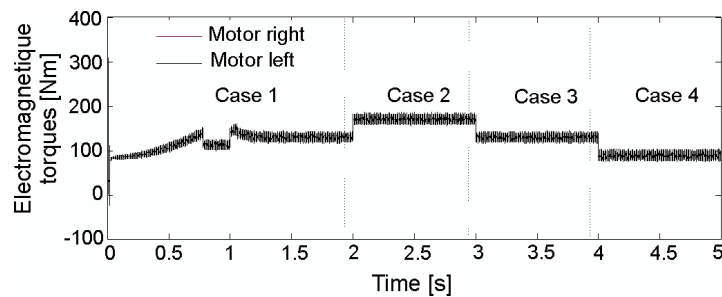


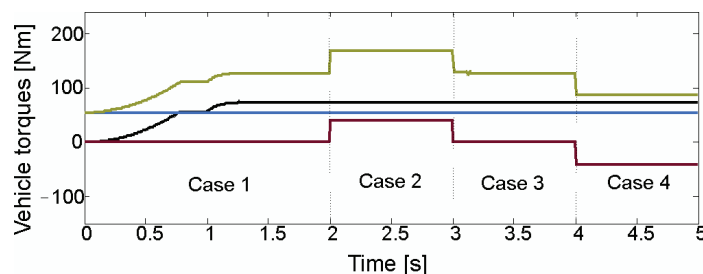Fig. 19. Variation of electromagnetic torques in different scenario.



Fig. 20. Evaluation of aerodynamic torque, rolling torque, slop torque and resistive vehicle torque

The comparative study for tow cases performance is shown in Table 4. In this paper we have presented comparative studies between MIMO-FLC and SISO-FLC speed controller. The MIMO-FLC controller method gives a satisfaction results for electric vehicle speed performance.

Table 4. Comparative study

| Parameter and indexes | MIMO-FLC | SISO-FLC |
|---|---|---|
| Aerodynamic torque [Nm] | 50.5470 | 51.0972 |
| Vehicle torque [Nm] | 89.55 | 88.99 |
| Current [A] | 54.11 | 54.93 |
| Electromagnetic torque [Nm] | 127.70 | 126.50 |

## 7. Conclusion

In this paper, the vehicle speed are controlled by multi-input multi-output fuzzy logic controller this paper has demonstrated the feasibility of an improved vehicle stability which utilizes two independent back drive wheels for motion by using DTC-SVM control. MIMO-FLC presented satisfactory performances and possesses good robustness (no overshoot, minimal rise time, Steady state error compared with SISO-FLC. This method has Improved EV steering and stability during different trajectory. The advantage of the proposed controller is its robustness and capacity to maintain ideal trajectories for two wheels control independently, also it can ensure good disturbance rejections with no overshoot and good stability of vehicle speed variation with less error. The DTC-SVM is more adaptive for propelled vehicle systems using independent wheel control with the ability to traverse steep slopes, to have larger wheels, improved load carrying and distribution of load compared to conventional vehicles of the same type. Using the proposed control method the electric vehicle has shown best comportment and stability during different road Path by maintaining the motorization error speed equal zero with a good deriving forces distribution. Finally, the simulation results showed clearly the performance of the proposed controller. The electric vehicle was proved an efficiency compartment in the different scenarios road constraints.

## Appendix

Table 5. Vehicle Parameters

| | | |
|---|---|---|
| $Te$ | Motor traction torque | 238 Nm |
| $J_e$ | Moment on inertia of the drive train | 7.07 Kgm$^2$ |
| $L_w$ | Distance between two wheels and axes | 2.5 m |
| $d_w$ | Distance between the back and the front wheel | 1.5 m |

Table 6. Induction Motors Parameters.

| | | |
|---|---|---|
| $R_r$ | Rotor winding resistance (per phase) | 0.0503 Ω |
| $R_s$ | Stator winding resistance (per phase) | 0.08233 Ω |
| $L_s$ | Stator leakage inductance (per pohase) | 724 μH |
| $L_m$ | Magnetizing inductance (per phase) | 0.0151 H |
| $L_r$ | Rotor leakage inductance (per phase) | 724 μH |
| $fc$ | Friction coefficient | 0.02711 |
| $P$ | Number of poles | 4 |

Table 7. Symbols, designation and units

| Symbols | Nomenclature | Units |
|---|---|---|
| $J_e$ | Moment of inertia of the drive train | Kg.m2 |
| $J_v$ | Vehicle inertia | Kg.m2 |
| $T_{em}$ | Electromagnetic torque | Nm |
| $T_v$ | Vehicle torque | Nm |
| $V_{dc}$ | Battery voltage | Volt |
| $\Delta\omega$ | Angular speed variation given by electronic differential | Rad/sec |
| $\omega_{mr}$ | Right wheel angular speed | Rad/sec |
| $\omega_{lr}^*$ | Left wheel angular speed | Rad/sec |
| $\omega_{mr}^*$ | Right wheel angular speed of reference | Rad/sec |
| $\omega_{lm}^*$ | Left wheel angular speed of reference | rad |
| $\delta$ | Reel angle wheel curve's | rad |

# References

[1] Yang Y.P., Lo C.P., *Current distribution control of dual directly driven wheel motors for electric vehicles*. Control Engineering Practice 16(11): 1285-1292 (2008).

[2] He P., Hori Y., Kamachi M. et al., *Future motion control to be realized by in-wheel motored electric vehicle*. In Proceedings of the 31st Annual Conference of the IEE Industrial Electronics Society, IEEE Press, Raliegh South Carolina, USA, pp. 2632-2637 (2005).

[3] Kang J.K., Sul S.K., *New direct torque control of induction motor for minimum torque ripple and constant switching frequency*. IEEE Trans. Ind. Applicat. 35(5): 1076-1082 (1999).

[4] Chan C.C. et al., *Electric vehicles charge forward*. IEEE Power Energy Mag. 2(6): 24-33 (2004).

[5] Zhu Z. et al., *Electrical machines and drives for electric, hybrid, and fuel cell vehicles*. Proc. IEEE 95(4): 764-765 (2007).

[6] Vas P., *Sensorless Vector and direct torque control*, Oxford University Press (1998).

[7] Itoh K., Kubota H., *Thrust ripple reduction of linear induction motor with direct torque control*. Proceedings of the Eighth International Conference on Electrical Machines and Systems, ICEMS 2005, 1: 655-658 (2005).

[8] Chen L., Fang K.L. *A novel direct torque control for dual-three-phase induction motor*, Conf. Rec. IEEE International Conference on Machine Learning and Cybernetics, pp. 876-888 (2003).

[9] Vas P., *Sensorless vector and direct torque control*. Oxford University Press, 1998.

[10] Schell A., Peng H., Tran D., Stamos E., *Modeling and control strategy development for fuel cell electric vehicle*. Annual Review in Control Elseiver 29: 159-168 (2005).

[11] Haddoun A., Modeling, *Analysis and neural network control of an EV electrical differentiel*. Transaction on Industriel Electronic 55(6), (2008).

[12] Nasri A., Hazzab A., Bousserhane I.K. et al., *Two wheel speed robust sliding mode control for electric vehicle drive.* Serbian Journal of Electrical Engineering 5(2): 199-216 (2008).

[13] Hartani K., *Electronic differential with direct torque fuzzy control for vehicle propulsion system.* Turk J. Elec. Eng. & Comp. Sci. 17(1), (2009), TUBITAK.

[14] Lam L.T., Lovey R., *Developpement of ultra-battery for hybrid-electric vehicle applications.* Elservier, power sources Vol. 158: 1140-1148 (2006).

[15] Larminie, *Electric vehicle technology explained.* John Wiley, John Lowry (ed.), England (2003).

[16] Haddoun A. et al., *Analysis modeling and neural network of an electric vehicle.* In: Proc IEEE IEMDC, Antalya Turky, pp. 854-859 (2007).

[17] Vasudevan M., Arumugam R., *New direct torque control scheme of induction motor for electric vehicles.* 5-th Asian Control Conference 2: 1377-1383 (2004).

[18] Benbouzid M.E.H. et al., *Advanced fault-tolerant control of induction motor drives for EV/HEV traction applications. From conventional to modern and intelligent control techniques.* IEEE Trans. Veh. Technol. 56(2): 519-528 (2007).

[19] Gupta A., Khambadkone A.M., *A space vector pwm scheme for multilevel inverters based on two-level space vector pwm.* IEEE Transaction on Industrial Electronics 53 (2006).

[20] Habetler T.G., Profumo F., Pastorelli M., Tolbert L. *Direct torque control of induction machines using space vector modulation.* IEEE Transaction on Industry Applications 28(5): 1045-1053 (1992).

[21] Holtz J., *Pulsewidth modulation for electronic power onversion.* Proceedings of the IEEE 82: 1194-1214 (1994).

[22] Zhou K. et al., *Relationship between space-vector modulation and three-phase carrier-based PWM: a comprehensive analysis.* IEEE Trans. Industrial Electronics 49(1): 186-195 (2002).

[23] Jun Fu T. et al., *Torque control of induction motors for hybrid electric vehicles.* Proceedings of the IEEE ACC'06, Minneapolis (USA), pp. 5911-5916 (2006).

[24] Zelechowski M. et al., *Controller design for direct torque controlled space vector modulation (DTC-SVM) induction motor drives.* Proceedings of the IEEE ISIE'05, Dubrovnik (Croatia), pp. 951-956 (2005).